Coexistence of Elastic Modulations in the Charge Density Wave State of 2*H*-NbSe$_2$

Bogdan Guster[1,#], Carmen Rubio-Verdú[2,#], Roberto Robles[1,#], Javier Zaldívar[2], Paul Dreher[3,4], Miguel Pruneda[1], José Ángel Silva-Guillén[5], Deung-Jang Choi[3,4,6], José I. Pascual[2,6], Miguel M. Ugeda*[2,3,4,6], Pablo Ordejón*[1] and Enric Canadell*[7]

[1]Catalan Institute of Nanoscience and Nanotechnology (ICN2), CSIC and BIST, Campus UAB, Bellaterra, 08193 Barcelona, Spain

[2]CIC nanoGUNE, 20018 San Sebastián, Spain

[3]Donostia International Physics Center (DIPC), Paseo Manuel de Lardizábal 5, 20018 San Sebastián, Spain

[4]Centro de Física de Materiales (CSIC-UPV-EHU), Manuel Lardizábal 5, 20018 San Sebastián, Spain.

[5]School of Physics and Technology, Wuhan University, Wuhan 430072, China

[6]Ikerbasque, Basque Foundation for Science, 48013 Bilbao, Spain

[7]Institut de Ciència de Materials de Barcelona (ICMAB-CSIC), Campus UAB, 08193 Bellaterra, Spain

Corresponding authors: pablo.ordejon@icn2.cat, canadell@icmab.es and mmugeda@dipc.org

[#] These authors contributed equally.

Abstract. Bulk and single-layer 2*H*-$NbSe_2$ exhibit identical charge density wave order (CDW) with a quasi-commensurate 3×3 superlattice periodicity. Here we combine scanning tunnelling microscopy (STM) imaging at $T = 1$ K of 2*H*-$NbSe_2$ with first-principles density functional theory (DFT) calculations to investigate the structural atomic rearrangement of this CDW phase. Our calculations for single-layers reveal that six different atomic structures are compatible with the 3×3 CDW distortion, although all of them lie on a very narrow energy range of at most 3 meV *per* formula unit, suggesting the coexistence of such structures. Our atomically resolved STM images of bulk 2*H*-$NbSe_2$ unambiguously confirm this by identifying two of these structures. Remarkably, these structures differ from the X-ray crystal structure reported for the bulk 3×3 CDW which, in fact, is also one of the six DFT structures located for the single-layer. Our calculations also show that due to the minute energy difference between the different phases, the ground state of the 3×3 CDW could be extremely sensitive to doping, external strain or internal pressure within the crystal. The presence of multi-phase CDW order in 2*H*-$NbSe_2$ may provide further understanding of its low temperature state and the competition between different instabilities.

Keywords: Charge density waves, transition metal dichalcogenides, DFT calculations, 2H-$NbSe_2$, STM.

Main text.

The genuine origin of the charge density wave (CDW) state in $NbSe_2$ has been a matter of continuous debate.[1,2] Clearing up this point is an unavoidable issue in any attempt to understand the interplay between CDW and superconducting (SC) states in this paradigmatic material.[3] Bulk 2*H*-$NbSe_2$ is a room temperature metal which at 33 K undergoes a transition towards an atypical CDW state[4] with practically no resistivity change through the transition. Below 33 K the system exhibits a modulated almost quasi-commensurate 3×3 structure[5] and at 7 K enters into a SC state[6]. It has been recently shown that the CDW order remains intact in single-layer $NbSe_2$[7]. In contrast with 2*H*-$NbSe_2$, the CDW modulation in bulk 2*H*-$TaSe_2$ is 3×3 commensurate at low temperature.[5] Dichalcogenides of the 2*H*-MX_2 family provide promising playground for the study of competing electronic instabilities in the 2D limit, 2*H*-$NbSe_2$ being specially challenging because of the incommensurability of its CDW.

Single-layers of 2*H*-$NbSe_2$ (from now on we will refer to them simply as $NbSe_2$) are hexagonal layers of Nb atoms in a trigonal prismatic environment of Se atoms (Figure 1a).[8] Although the superlattice periodicity (quasi-commensurate 3x3) has been accurately measured,[5] the microscopic structure of the elastic distortion that accompanies the CDW phase still remains elusive. The layers of bulk 2H-$NbSe_2$ were recently found to exhibit a continuous pattern of overlapping star-shaped Nb atom clusters extending along the layer.[9] More recently, a first-principles DFT study on single-layer $NbSe_2$ assuming a commensurate 3×3 modulation revealed that several structures with nearly equal stability but different distortion patterns are compatible with a 3×3 modulation.[10] This suggests a very flat potential energy surface and a plausible coexistence of the different modulations. This potentiality apparently stimulated two subsequent theoretical works.[11,12] However, a comprehensive picture of the exact elastic modulations cannot be solved from a purely theoretical DFT approach since (i) the real modulation is strictly non-commensurate, and (ii) the resulting competing modulations have very similar energetic stability. Because of the simultaneous occurrence of these two features, theoretically optimized 3×3 commensurate structures can only be taken as suggestions of different possibilities to be carefully examined by suitable experimental techniques. STM well suits for this purpose since it can image with atomic resolution the spatial rearrangement of the electronic charge of the CDW phase. Such electronic rearrangements can be compared to those simulated for the different calculated elastic modulations. Here we report a combined experimental-theoretical study to provide compelling evidence for the coexistence of different modulations in the CDW state of $NbSe_2$. In order to search for the several possible competing phases, we perform total energy minimizations starting from different distorted starting configurations. Some of the structures were only found when a charge doping was initially considered. Once such structures are located for a given doping value, their evolution with doping was also followed. While some of the phases were found for the whole range of doping considered, others were observed for some doping intervals. Doping is therefore used as a practical way to unravel competing structures in our calculations. Nevertheless, we note that our results of the stability of the several structures as a function of doping can also be relevant to experiments where injection of carriers in the single layers is achieved through electric field gating.[13] We also note again that our commensurate 3×3 structural models are only (close) approximations to the true experimental incommensurate structures.

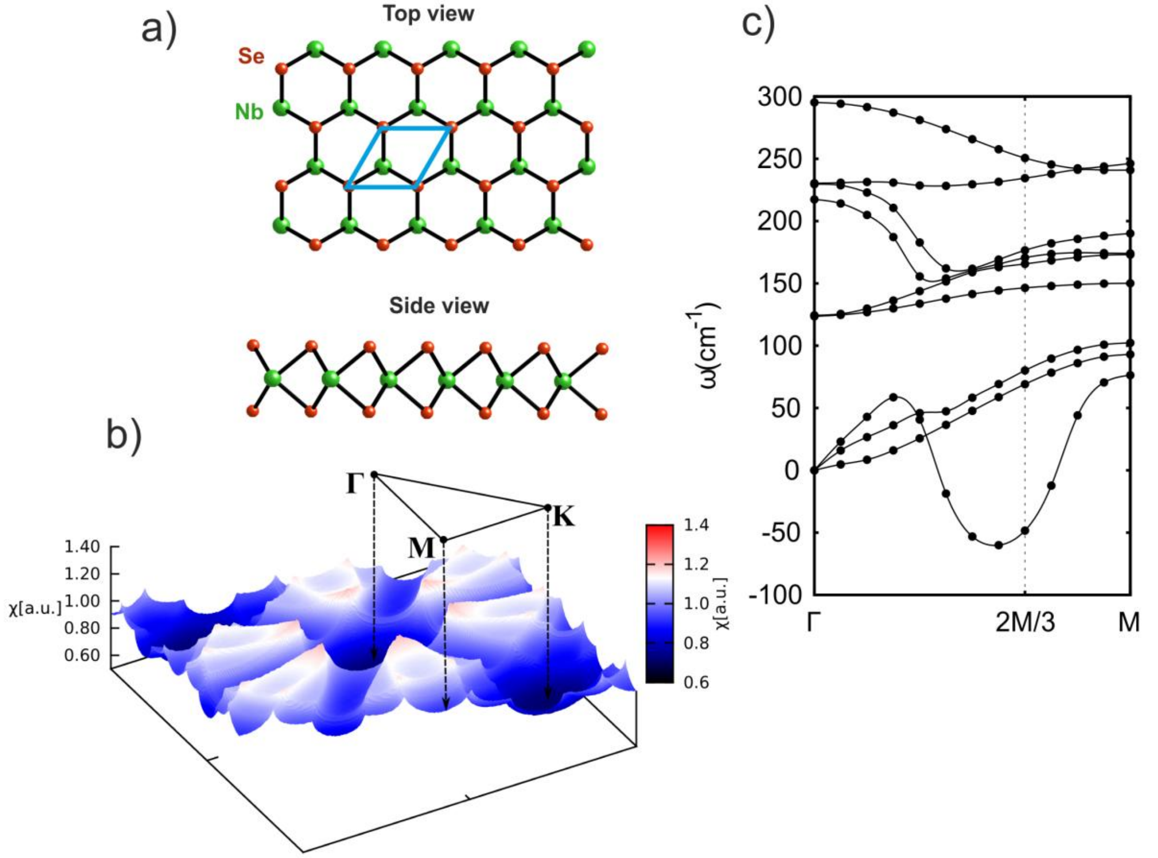

Figure 1: (a) Top and side view of the NbSe$_2$ single-layer structure. Lindhard response function (b) and (c) phonon dispersion in the Γ - M segment of the Brillouin zone calculated for undistorted single-layer NbSe$_2$.

Full optimization of the non-modulated structure of single-layer NbSe$_2$ leads to a lattice constant of 3.48 Å, in good agreement with plane-wave type DFT studies,[11] 3.47 Å, and the experimental value for the bulk, 3.44 Å.[8] The band structure and Fermi surface of single-layer $NbSe_2$ in both modulated[10-12] and non modulated[14-16] structures have been discussed before. Such Fermi surface contains rounded hexagons and rounded triangles centered at Γ and K points of the Brillouin zone (BZ), respectively. The calculated Lindhard response function for the optimized non modulated single-layer $NbSe_2$ is shown in Figure 1b. As it occurs for the bulk,[17] there are no sharp maxima around the ($a^*/3$, 0) point and equivalent ones of the BZ which could justify a Fermi surface nesting driven mechanism of the CDW, but a very shallow region around the Γ - M direction. In contrast, as can be seen in the phonon band structure of the optimized non modulated structure shown in Figure 1c, one of the phonon branches becomes clearly unstable in a large part of the Γ-M segment of the BZ, with a maximum imaginary frequency near but not exactly at the $a^*/3$ point. The presence of phonons with imaginary frequency around this point indicates that the system is unstable with respect to incommensurate distortions with a periodicity not far from 3×1 (and symmetry equivalent). The combination of the three equivalent distortions (threefold symmetry, i.e. triple-q or 3Q mechanism), leads to an incommensurate structure close to 3×3. We conclude that the modulation of the single-layer $NbSe_2$ is a strong-coupling CDW caused by electron-phonon coupling, as it has been proposed for the bulk[16] and we previously discussed for single-layers.[10]

We then performed structural optimizations imposing a 3×3 periodicity for the pristine as well as for several doping levels of single-layer $NbSe_2$. We also checked that the phonon instability remains under doping: as we show in the Supplementary Information, the effect of doping does not change this picture qualitatively, although the precise shape of the unstable phonon branch and the position of the minimum experience some small changes. A summary of this study is reported in Figure 2. Up to six different modulations compatible with a 3×3 cell were found. One of the structures exhibits centered hexagonal clusters of Nb atoms and single Nb atoms in between (noted Hexagons in Figure 2). Another structure contains a continuous pattern of overlapping star-shaped Nb atom clusters (noted Stars in Figure 2) which coincides with the 3×3 modulation reported for the bulk.[9] Two structures contain triangular clusters of 3 and 6 Nb atoms (T1 and T1' in Figure 2) but whereas in T1 the inner triangles of both clusters are centered by two Se atoms above and below the Nb atoms plane, in T1' they are centered by hollows. Finally, two more structures contain a continuous pattern of overlapping triangular clusters of 6 Nb atoms of two different types, with or without Nb-Nb short distances inside the large triangles (T2 and T2’ in Figure 2). Note that the six structures can be paired in three groups: Hexagons/Stars, T1/T2 and T1’/T2’ so that within each pair the short and long Nb-Nb bonds are interchanged. This suggests that the two structures within each pair may be interconverted as a function of doping. This is indeed the case for the T1/T2 and T1’/T2’ pairs where a relatively simple gradual change between the two structures is possible. However, the Hexagons/Stars pair could not be exchanged due to their complex arrangement. Consequently, for a given carrier-density there are four different structures compatible with a 3×3 modulation. Remarkably, for most doping levels the energy difference between these structures is extremely small (between fractions of a meV and at most 2 meV) so that it is likely that some of the structures experimentally coexist. Let us stress that our calculations are carried out for a commensurate 3×3 CDW structure but the real modulation is incommensurate. As a consequence of this fact and the very small energy differences, the data in Figure 2a should be only taken as suggesting that some of these structures may coexist in real samples and weak changes in doping, strain or internal pressure of the crystal may alter such coexistence.

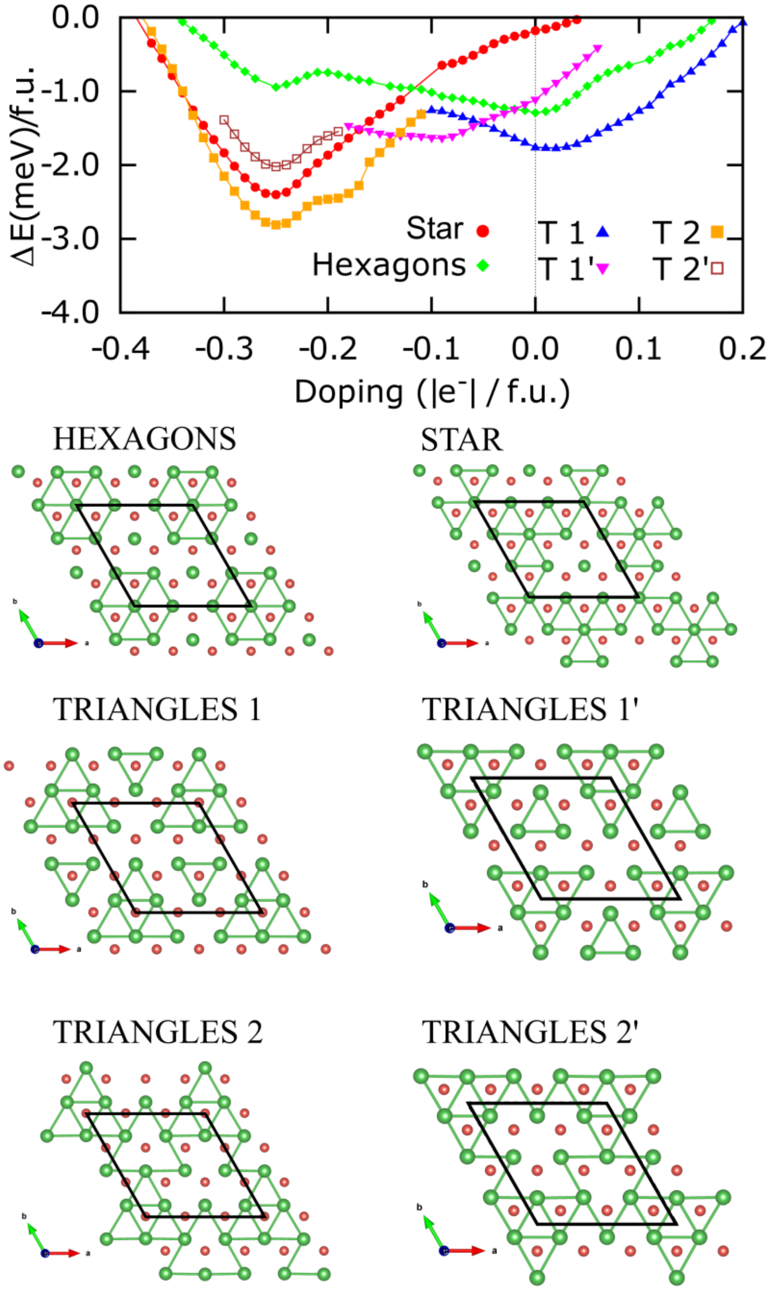

Figure 2: Different modulations compatible with a 3×3 periodicity and their relative energies for single-layer $NbSe_2$ as a function of external doping (in electrons per formula unit; negative values indicate electron doping). For a given doping value the energy (in meV *per* formula unit) is given with respect to the optimized non distorted system for the same doping level. Nb-Nb contacts shorter than in the average structure are those shown in the structural drawings. Nb-Nb bonds smaller than the lattice constants are marked with green lines to visualize the different modulations.

We have performed the analysis of the stability of the six different structures with 3×3 periodicity by obtaining the phonon frequencies. As some of the phases are only stable under charge doping, the frequencies were obtained using two doping values: 0 and -0.25 e/f.u. For no doping, we find that the hexagons, T1 and T1' structures are stable and show no imaginary frequencies, while the stars phase does show three imaginary frequencies, in agreement with the previous works.[11,12] For the case of -0.25 e/f.u. doping, we find that the T2, T2' and stars phases are stable, while the hexagons phase has three imaginary frequencies. We note that this is consistent with the energy ordering of the phases as a function of doping in Figure 2: the phases which are found to have unstable modes are the ones with higher energies (stars for zero doping, and hexagons for -0.25 e/f.u. doping).

In order to experimentally explore the existence of these structural phases, we have imaged the surface of bulk 2*H*-$NbSe_2$ with atomic resolution by means of scanning tunnelling microscopy (STM) at T = 1 K. Since both bulk and single-layer $NbSe_2$ exhibit the same 3×3 CDW phase,[7] we carried out our experiments in its bulk form due to the its much lower density of defects (grain boundaries and domain edges are not present in bulk), which might alter the energy landscape of the CDW phases. Furthermore, the purely two dimensional character of the CDW order in $NbSe_2$ allows us to directly probe the existence of the structural phases predicted for single-layer $NbSe_2$ in the bulk form. The analysis of tens of different regions of bulk $NbSe_2$ led to identification of two different structural phases. Upper panel in Figure 3 shows two STM images of a representative region for unoccupied (Figure 3a) and occupied (Figure 3b) states. The STM images reveal the coexistence of two different phases (depicted in blue/yellow) separated by an Å-scale boundary (black dashed line). Although the two phases show the same 3×3 superlattice periodicity at both polarities, the relative intensity of the nine Se atoms of each 3×3 unit cell (blue and yellow cells) vary differently, thus giving rise to a unique pattern in each case. Figures 3c-f show close-up views of these patterns for the two phases at each polarity. Such unique patterns allowed us to compare both structural phases with simulated STM images from the six stable structures, within the Tersoff-Hamann approximation pattern (see the Supplementary Information for the images of the Hexagons, Stars and T1’ phases not shown in Figure 3).[18] As a first result, the experimental phase labelled in blue can be identified with the theoretical T2'. Figures 3g and 3i show the simulated STM images of this phase at ± 0.05 V that compare with the experimental STM images in Figures 3c and 3e, respectively. The theoretical 3×3 unit cells reproduce the relative intensity of the Se atoms within the unit cells simultaneously for both polarities as well as their relative orientation. Regarding the yellow phase, it can be identified with either the T1 or T2 phases since they exhibit almost the same patterns at both polarities and, therefore, are practically indistinguishable. Figures 3h and 3j show the simulated STM images for the T1 phase at ± 0.05 V (those for T2 are almost identical) for comparison with the experimental ones in Figures 3d and 3f, respectively. Here, again, the patterns within the 3×3 unit cells show a good agreement between theory and experiment. We therefore assign the observed yellow (blue) phases to the T2' and T1/T2 phases. Although this is the most likely correspondence between the experimental and theoretical phases, the blue phase can also be identified as the Stars phase according to the superlattice. However, this would imply a rotation of 180° of the crystal lattice with respect to the T1/T2 phase and, therefore, their mutual coexistence is not compatible in light of the experimental data.

In summary, on the basis of first-principles DFT calculations six different structures are found to be compatible with the 3×3 CDW structure of $NbSe_2$. All these structures are found to coexist in a very narrow energy range of 2-3 meV. Their relative stability can be subtly altered by doping or strain. Imaging the surface of bulk 2*H*-$NbSe_2$ with atomic resolution allowed us to identify two of these structures, as anticipated by our theoretical simulations. Intriguingly, these structures differ from the X-ray crystal structure reported for the bulk 3×3 CDW [9] which, in fact, is also one of the six DFT structures located for the single-layer (Stars in Figure 2). Preliminary calculations for slabs with a different number of layers suggest that the actual structure stabilized may change from layer to layer, i.e., the energetic preference may depend also on the internal pressure. The coexistence of different structures in 2*H*-$NbSe_2$ has far-reaching consequences to fully understand the electronic ground state of 2*H*-$NbSe_2$. Thus, experimental work on slabs with different number of layers is encouraged since it may provide important clues to understand the puzzling physics of this correlated material.

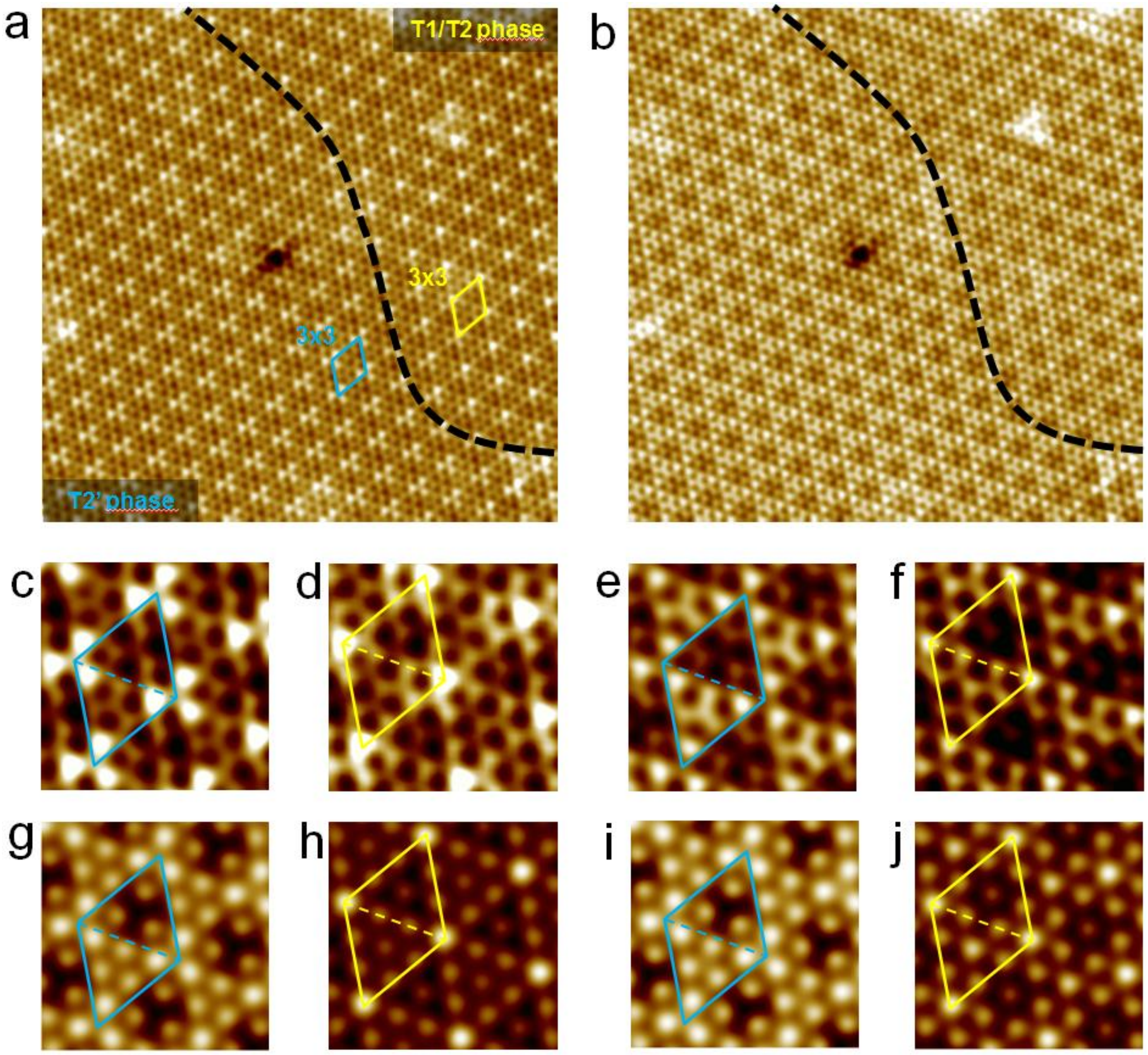

Figure 3. Unoccupied [+50 mV] (a) and occupied [-50 mV] (b) STM images (14 nm x 14 nm) of the same region of bulk 2*H*-NbSe$_2$ showing the coexistence of two structural phases. The black dashed line represents the boundary between them. Parameters: (a) $V_S = 50$ mV, I = 0.5 nA and (b) $V_S = -50$ mV, I = 0.5 nA. (c-f) Zoom-in STM images from **a** and **b** of the two phases for unoccupied (c,d) and occupied (e,f) states. (g-j) Simulated STM images for both phases and bias polarities ($V_S = \pm 50$ mV).

Computational details. The geometrical optimizations, electronic and phonon band structures were carried out with density functional theory (DFT)[19,20] using a numerical atomic orbitals approach implemented in the SIESTA code.[21,22] We used the Perdew-Burke-Ernzerhof (PBE) functional to account for the exchange-correlation energy.[23] A split-valence double-ζ basis set[24] was used to describe the valence electrons wave function, while the core electrons were replaced by norm conserving scalar relativistic pseudopotentials[25] factorized in the Kleinman-Bylander form.[26] The 4p shell of Nb was included in the valence explicitly as semicore states. For a good description of the free standing layer, we placed the single layer in a vacuum space of 50 Å to avoid interactions between the layer and its images. We used an energy cutoff of 2500 Ry for the real space integration. A tolerance of 10^{-5} and 10^{-4} on the density matrix and total energy, respectively, was used in order to attain the convergence of the self-consistency cycle. Geometrical optimization calculations were performed to ensure a maximum atomic force of 4×10^{-3} eV/$Å^{-1}$. A Monkhorst-Pack[27] *k*-point grid of 72×72×1 was used to account for the sampling of the Brillouin zone of the minimum unit cell and it was scaled accordingly where supercell calculations were performed. Phonon calculations were done using the finite difference method. In the case of the phonon band structure calculations, a *k*-point grid of 120×120×1 per minimum unit cell and a 5×10^{-3} eV Fermi-Dirac smearing were used.

Experimental details. Bulk $NbSe_2$ crystals were cleaved under Ultra-High Vacuum (UHV) conditions, and subsequently transferred *in-situ* into a SPECS GmbH Low-Temperature STM for imaging at T = 1.2 K. STM/STS analysis and rendering was done using the WSxM software.[28]

ORCID

Bogdan Guster: 0000-0003-1305-1862
Roberto Robles: 0000-0001-7808-0395
Enric Canadell: 0000-0002-4663-5226
Pablo Ordejón: 0000-0002-2353-2793
José Ángel Silva-Guillen: 0000-0002-0483-5334
José Ignacio Pascual: 0000-0002-7152-4747

Notes

The authors declare no competing financial interest.

Acknowledgements. Work at Bellaterra was supported by Spanish MINECO (Grants FIS2015-64886-C5-3-P and FIS2015-64886-C5-4-P, and the Severo Ochoa Centers of Excellence Program under Grants SEV-2017-0706 and SEV-2015-0496), Generalitat de Catalunya (Grant 2017SGR1506 and the CERCA Program) and by the European Union MaX Center of Excellence (Grant No. 824143). The work by BG has been performed in the context of the Physics PhD program of the Universitat Autònoma de Barcelona. M.M.U acknowledges support by the Spanish MINECO under grant no. MAT2017-82074-ERC and by the ERC Starting grant "LINKSPM" (Grant No. 758558).

References

1. Rossnagel, K. On the origin of charge-density waves in select layered transition-metal dichalcogenides. *J. Phys.:Cond. Matt*. **2011**, *23*, 213001.
2. Zhu, X.; Cao, Y.; Zhang, J.; Plummer, E. W.; Guo, J. Classification of charge density waves based on their nature. *Proc. Nat. Acad. Sci. USA* **2018**, *112*, 2367.
3. Castro Neto, A. H. Charge Density Wave, Superconductivity, and Anomalous Metallic Behavior in 2D Transition Metal Dichalcogenides. *Phys. Rev. Lett*. **2001**, *86*, 4382.
4. Wilson, J.; Di Salvo, F.; Mahajan, S. Charge-density waves and superlattices in the metallic layered transition metal dichalcogenides. *Adv. Phys*. **1975**, *24*, 117-201.
5. Moncton, D. E.; Axe, J. D.; DiSalvo, F. J. Neutron scattering study of the charge-density wave transitions in 2H-$TaSe_2$ and 2H-$NbSe_2$. *Phys. Rev. B* **1977**, 16, 801.
6. Revolinsky, E.; Lautenschlager, E. P.; Armitage, C. H. Layer structure superconductor. *Solid State Comm*. **1963**, *1*, 59-61.
7. Ugeda, M. M. ; Bradley, A. J.; Zhang, Yi; Onishi, S.; Chen, Yi; Ruan, W.; Ojeda-Aristizabal, C.; Ryu, H.; Edmons, M. T.; Tsai, H.-Z.; Riss, A.; Mo, S.-K.; Lee, D.; Zettl, A.; Hussain, Z.; Shen, Z.-X.; Crommie, M. F. Characterization of collective ground states in single-layer $NbSe_2$. *Nature Phys*. **2016**, *12*, 92.

8. Meerschaut, A.; Deudon, C. Crystal structure studies of the 3R-$Nb_{1.09}S_2$ and 2H-$NbSe_2$ compounds: correlation between nonstoichiometry and stacking type (= polytypism). *Mat. Res. Bull*. **2001**, *36*, 1721-1727.
9. Malliakas, C. D.; Kanatzidis, M. G. Nb-Nb Interactions Define the Charge Density Wave Structure of 2H-$NbSe_2$. *J. Am. Chem. Soc*. **2013**, *135*, 1719-1722.
10. Silva-Guillén, J. A.; Ordejón, P.; Guinea, F.; Canadell, E. Electronic structure of 2H-$NbSe_2$ single-layers in the CDW state. *2D Materials* **2016**, *3*,035028.
11. Zheng, F.; Zhou, Z.; Liu, X.; Feng, J. First-principles study of charge and magnetic ordering in monolayer $NbSe_2$. *Phys. Rev. B* **2018**, *97*, 081101(R).
12. Lian, C.-S.; Si, C.; Duan, W. Unveiling Charge-Density Wave, Superconductivity, and Their Competitive Nature in Two-Dimensional $NbSe_2$. *Nano Lett*. **2018**, *18*, 2924.
13. Note that doping of transition metal dichalcogenide single-layers can also be achieved by growing the single-layers on a Au(111) substrate: (a) Sanders, C. E.; Dendzik, M.; Ngankeu, A. S.; Eich, A.; Bruix, A.; Bianchi, M.; Miwa, J. A.; Hammer, B.; Khajetoorians, A. A.; Hofmann, P. Crystalline and electronic structure of single-layer TaS_2. *Phys. Rev. B* **2016**, *94*, 081404; (b) Albertini, O. R.; Liu, A. Y. ; Calandra, M. Effect of electron doping on lattice instabilities in single-layer 1H-TaS_2. *Phys. Rev. B* **2017**, *95*, 235121.
14. Kim, S.; Son, Y.-W. Quasiparticle energy bands and Fermi surfaces of monolayer $NbSe_2$. *Phys. Rev. B* **2017**, *96*, 155439.
15. Lebègue, S.; Eriksson, O. Electronic structure of two-dimensional crystals from *ab initio* theory. *Phys. Rev. B* **2009**, *79*, 115409.
16. Calandra, M.; Mazin, I. I.; Mauri, F. Effect of Dimensionality on the charge-density wave in few-layer 2H-$NbSe_2$. *Phys. Rev. B* **2009**, *80*, 241108.
17. Johannes, M. D.; Mazin, I. I.; Howells, C. A. Fermi-surface nesting and origin of the charge-density wave in $NbSe_2$. *Phys. Rev. B* **2006**, *73*, 205102, and references therein.
18. Tersoff, J.; Hamman, D. R. Theory and Application for the Scanning Tunneling Microscope. *Phys. Rev. Lett*. **1983**, *50*, 1998.
19. Hohenberg, P.; Kohn, W. Inhomogeneous Electron Gas. *Phys. Rev*. **1964**, *136*, B864-B871.

20. Kohn, W.; Sham, L. J. Self-Consistent Equations Including Exchange and Correlation Effects. *Phys. Rev*. **1965**, *140*, A1133-A1138.
21. Soler, J. M.; Artacho, E.; Gale, J. D.; García, A.; Junquera, J.; Ordejón, P.; Sánchez-Portal, D. The SIESTA method for ab initio order-N materials simulation. *J. Phys.: Cond. Matt*. **2002**, *14*, 2745-2779.
22. Artacho, E.; Anglada, E.; Diéguez, O.; Gale, J. D.; García, A.; Junquera, J.; Martin, R. M.; Ordejón, P.; Pruneda, J. M.; Sánchez-Portal, D.; Soler, J. M. The SIESTA method: developments and applicability. *J. Phys. Cond. Matter* **2008**, *20,* 064208.
23. Perdew, J. P.; Burke, K.; Ernzerhof, M. Generalized Gradient Approximation Made Simple. *Phys. Rev. Lett*. **1996**, *77,* 3865-3868.
24. Artacho, E.; Sánchez-Portal, D.; Ordejón, P.; García, A.; Soler, J. M. Linear Scaling ab-initio Calculations for Large and Complex Systems. *Phys. Status Solidi B* **1999**, *215,* 809-817.
25. Troullier, N.; Martins, J. L. Efficient Pseudopotentials for plane-wave calculations. *Phys. Rev. B* **1991**, *43*, 1993-2006.
26. Kleinman, L.; Bylander, D. M. Efficacious Form for Model Pseudopotentials. *Phys. Rev. Lett*. **1982**, *48*, 1425-1428.
27. Monkhorst, H. J.; Pack, Special points for Brillouin zone integrations. J. D. *Phys. Rev. B* **1976**, *13*, 5188-5192.
28. Horcas, I.; Fernández, R. WSXM: A software for scanning probe microscopy and a tool for nanotechnology. *Rev. Sci. Instrum.* **2007**, *78*, 013705.

For the Table of Contents